Computationally Efficient Strategy for Modeling the Effect of Ion Current Modifiers

David G. Rand, Qinlian Zhou, Gregery T. Buzzard, Jeffrey J. Fox

***Abstract*—Electrophysiological studies often seek to relate changes in ion current properties caused by a chemical modifier to changes in cellular properties. Therefore, quantifying concentration-dependent effects of modifiers on ion currents is a topic of importance. In this study, we sought a mathematical method for using ion current data to predict the effect of several theoretical ion current modifiers on cellular and tissue properties that is computationally efficient without compromising predictive power. We focused on the K^+ current $I_{K,r}$ as an example case due to its link to long QT syndrome and arrhythmias, but these methods should be generally applicable to other electrophysiological studies. We compared predictions using a Markov model with mass action binding of the modifiers to specific conformational states of the channel to predictions generated by two simplified models. We investigated scaling $I_{K,r}$ conductance, and found that although this method produced predictions that agreed qualitatively with the more complicated model, it did not generate quantitatively consistent predictions for all modifiers tested. Our simulations showed that a more computationally efficient Hodgkin-Huxley model that incorporates the effect of modifiers through functional changes in the current produced quantitatively consistent predictions of concentration-dependent changes cell and tissue properties for all modifiers tested.**

***Index Terms*—Computer simulation, electropharmacology, electrophysiology, mathematical modeling**

I. Introduction

MATHEMATICAL modeling and computational simulations have a long history of use in electrophysiology, dating back to the seminal work of Hodgkin and Huxley [1]. One of the primary questions that mathematical tools have been used to address is how ion currents that flow through a variety of types of ion channels control the membrane potential to generate the rich dynamics that are observed in cells [2]. For example, the electrical behaviors exhibited by cells can include oscillations in cardiac pacemaker cells [3] and neurons [4], bursting in pancreatic B-cells [5], and excitability in cardiac ventricular cells [6] and Purkinje fibers [7]. The rapid increase and subsequent return to rest of the membrane potential in excitable and oscillatory cells is often called an action potential (AP).

Mathematical models have been used to explain cellular behaviors such as the AP in terms of the dynamics of the important ion currents in each cell type [8]. An important feature of many of these models is that the conductance of a particular ion channel can be time and voltage dependent [2].The change in conductance of an ion channel is often modeled as a set of nonlinear differential equations describing the opening and closing of one or more independent gates, following the formalism introduced by Hodgkin and Huxley [1]. An alternative description called a Markov gating model describes voltage-dependent transitions between discrete states that correspond to different physical conformations of the channel proteins [9].

Often electrophysiologists are interested in studying the response of cellular electrical activity to a perturbation in the cellular environment. For example, a researcher might wish to observe the response of a single (or multiple) ion current(s) to a chemical that modifies the properties of that current, and then to relate the changes in the current to changes in cellular behavior. Some particularly important electrophysiological modifiers include natural toxins [10], drugs designed to treat central nervous system disorders [11], cellular kinases that phosphorylate channels [12], and second messenger molecules such as Ca^{2+} ions [13] and cAMP [14] that are used to relay important cellular signals. In addition, some compounds that are designed to treat disorders from a wide range of therapeutic areas have been found to interrupt the normal activity of cardiac ion currents in potentially dangerous ways [15]. One ion current in particular, the delayed rectifier potassium current $I_{K,r}$ that results from expression of the HERG gene, appears to be an unwanted target of many compounds that have been shown to induce abnormal cardiac rhythms [16], including a dangerous and potentially fatal arrhythmia called Torsades de Pointes [15]. Quantifying the effects of ion current modifiers on the electrical properties of individual ion currents and on cellular properties could help electrophysiologists understand why certain compounds might

Manuscript received September 12, 2006. This work was supported by NIH Grant R43 HL077938, NIH Grant R01 HL075515, NIH Grant R43 HL081687, NIH Grant R43 HL079709, and NSF Grant DMS-0408293. .

D. G. Rand was with Gene Network Sciences, 53 Brown Road, Ithaca NY 14850 USA. He is now with the Department of Systems Biology, Harvard University, Cambridge, MA 02115 USA (email: drand@fas.harvard.edu)

Q. Zhou is with Gene Network Sciences, 53 Brown Road, Ithaca NY 14850 USA (email: qzhou@gnsbiotech.com)

G. T. Buzzard is with the Department of Mathematics, Purdue University, West Lafayette, IN 47907 USA (email: buzzard@math.purdue.edu)

J. J. Fox is with Gene Network Sciences, 53 Brown Road, Ithaca NY 14850 USA (phone: 607-257-0332; fax: 607-257-5428; email: jeff@gnsbiotech.com).

induce harmful, or helpful, changes in ion currents and cellular behaviors.

Several experimental methods exist for measuring the effect of a modifier on an ion channel, including voltage clamp assays, binding assays, and fluorescence assays [17]. Voltage clamp assays involve measurements of current generated in response to voltage command protocols in isolated cells. Change in normalized peak current in response to voltage clamp stimulation using voltage step command protocols [18-20] or AP command protocols [20-23] is often used to measure the effect of the modifier on the current.

Ideally, the results of an experimental characterization of a modifier's effect on an ion current could be used to predict likely changes in cellular and tissue electrophysiological properties. To predict changes in cellular or tissue properties based on ion current data, it is necessary to incorporate concentration-dependent effects of the modifier into an accurate model of the ion current. Furthermore, it is desirable to minimize the complexity of the model so as to reduce the computational resources necessary to fit the model to data.

A common method for modeling the effect of a modifier on an ion current is to fit the normalized peak current concentration-response data to a standard sigmoid curve. In this case, the half-maximal response parameter, the EC_{50} (or IC_{50} for ion current inhibitors) can be used to quantify the modifier's effect on the ion current. While this method has the advantage of simplicity, it has been shown that the measured value of this parameter can depend on the experiment that is used to measure the effect of the modifier on the current. For example, some compounds that inhibit $I_{K,r}$ have been shown to have different IC_{50} values when the $I_{K,r}$ current is measured under different stimulus patterns [24].

Another more complicated method used to model the effect of a modifier involves constructing Markov state transition models of the binding of the modifying compound to the ion channel [25]. Models constructed according to this formalism attempt to reflect the physical interaction of the ion channel and the modifier under study. This method often uses prior knowledge of the binding properties of the modifier to reduce the number of unknown parameters. Alternatively, modeling the effect a novel modifier with unknown binding properties requires the estimation of a large number (which can increase quickly depending on the complexity of the modifier/ion channel interactions) of parameters. Consequently, a method that is less computationally intensive but has equal predictive power would be highly advantageous.

In this study, we sought an approach for mathematically modeling the effect of a modifier on an ion current that produces quantitative predictive agreement with a Markov model without requiring either prior knowledge of the physical properties of the modifier or extensive computation. Such a model could be used to predict changes in cellular and tissue properties as a function of modifier concentration for novel compounds based on experimentally collected ion current concentration-response data. To evaluate models of the effect of the modifier in this study, we modeled binding of compounds that block $I_{K,r}$. This ion current was chosen because it has been extensively studied due to its association with the lengthening of the QT interval of the electrocardiogram (ECG) and life-threatening cardiac arrhythmias such as Torsades de Pointes (TdP) [15]. Although the exact mechanism by which an $I_{K,r}$ blocker may induce TdP remains unknown, the arrhythmogenic properties of such modifiers have been hypothesized to involve the amplification of intrinsic electrical heterogeneity in the ventricular tissue, caused by preferential prolongation of the midmyocardial (M) cell action potential duration (APD) relative to epicardial and endocardial cell APD [26]. Thus, $I_{K,r}$ represents an ideal current for use in developing a method for incorporating concentration-dependent effects of an ion current modifier. However, the method developed in this work is general and does not depend on the details of this particular current.

Using a Markov model with direct binding of the modifier, we created three theoretical modifiers and generated synthetic ion current data and APD concentration-response predictions for each. We then used these data to evaluate two alternate modeling methods for quantifying modifier-ion channel interactions, the commonly used method of scaling channel conductance as a function of concentration [19, 27] in a Markov model, and a novel method involving a Hodgkin-Huxley (HH) formulation. Previous work has related Markov and HH models by incorporating knowledge of a modifier's binding properties [28], but the method described here requires no such prior knowledge.

II. Methods

To study modifier-ion current interactions, we modeled the canine rapid inward delayed rectifier K^+ current $I_{K,r}$, and its interaction with three theoretical modifiers, using three different mathematical formulations. First, we used a deterministic Markov model with mass action binding kinetics ($Markov_{MB}$) to simulate the effect of modifiers that bind to particular states of the channel. Next, we used the same Markov control model of $I_{K,r}$ and replaced mass action kinetics with scaling of channel conductance to model the effect of the modifier ($Markov_{GKr}$). Lastly, we studied a method for using a Hodgkin-Huxley (HH) model with modifier dependence (HH_{Mod}) as a framework for determining the functional consequences of the modifier-ion current interaction, such as changes in conductance, or activation and inactivation kinetics.

2.1.1 $Markov_{MB}$ model topology

The Markov model we studied follows the five state formulation given in Mazhari et al 2001 [9], with three closed states (C_1, C_2, and C_3), one open state (O), and one inactive state (I). We examined the effect of three theoretical modifiers that preferentially bind a single conformational state of the $I_{K,r}$ channel (Figure 1; modifiers binding states C_1 and C_2

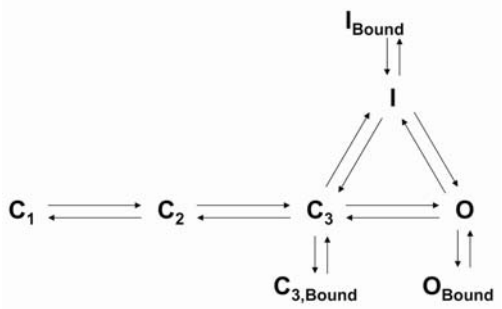

Fig. 1. State diagram of the $I_{K,r}$ Markov model with modifier binding. C_1, C_2, and C_3 are closed states, O is the open state, and I is the inactive state. Each Y_{bound} state is a modifier-channel complex with the channel in state Y. Transitions from state to state are functions of voltage of the form A*exp(B*V), and modifier binding and unbinding rates are voltage independent functions of modifier concentration and state occupancy. $I_{K,r}$ is a function of the population of state O.

produced similar results to the modifier binding state C_3 and are therefore not discussed in the text). Mass-action kinetics was used to model binding and unbinding of a modifier to a given state of the Markov model, with each modifier assigned a binding rate, k_{on}, and an unbinding rate, k_{off} (see Section 2.1.2). Although this model is a simplification of the physiological reality, it still allows for interesting and non-intuitive dynamics.

This formulation assumes that when a modifier binds a given conformational state, the channel cannot transition to a different conformational state until the modifier unbinds. That is, there are no transitions between bound states of the model (i.e. I_{Bound} -> O_{Bound}), only between bound and unbound states (i.e. I_{Bound} -> I -> O -> O_{Bound}). This approximation is valid for preferential binding of a single state as long as k_{on}(preferred state) >> k_{on}(other states) and k_{off}(preferred state) >> k_{off}(other states). Additionally, this model assumes that no current flows through the open state O when bound by $Modifier_O$.

2.1.2 Choice of parameters

To facilitate the study of the $I_{K,r}$ Markov model in computer simulations of canine ventricular APs, transition rate parameters in the Markov model were chosen to qualitatively reproduce canine $I_{K,r}$ recordings from previous experiments [29]. Transition rates for the control model are shown in

TABLE I
TRANSITION RATES FOR MARKOV MODEL OF $I_{K,R}$

$C_1 \rightarrow C_2$	$\alpha_0 = 0.00414573 \times \exp(0.09856 \times V)$
$C_2 \rightarrow C_1$	$\beta_0 = 0.00291266 \times \exp(-0.0315044 \times V)$
$C_3 \rightarrow O$	$\alpha_1 = 0.000586909 \times \exp(0.0170419 \times V)$
$O \rightarrow C_3$	$\beta_1 = 0.000232786 \times \exp(-0.0567021 \times V)$
$O \rightarrow I$	$\alpha_i = 0.927666 \times \exp(0.0186985 \times V)$
$I \rightarrow O$	$\beta_i = 0.0138023 \times \exp(-0.0252146 \times V)$
$C_3 \rightarrow I$	$\alpha_{i3} = 0.00707894 \times \exp(3.49E\text{-}08 \times V)$
$I \rightarrow C_3$	$\psi = (\beta 1 \times \beta i \times \alpha i 3)/(\alpha 1 \times \alpha i)$
$C_2 \rightarrow C_3$	$K_f = 0.0441566$
$C_3 \rightarrow C_2$	$K_b = 0.272749$

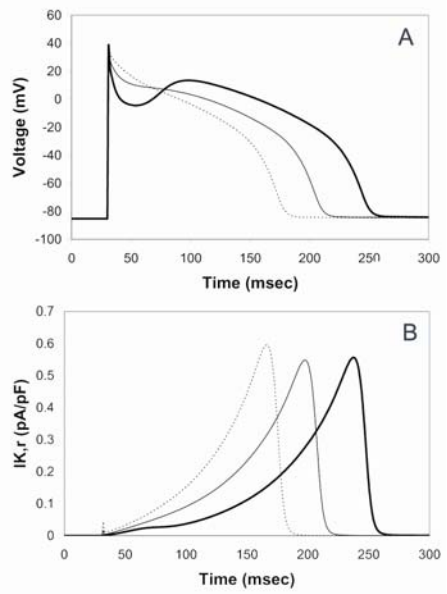

Fig. 2. A, AP clamp command APs at 1000 msec (thick line), 500 msec (thin line), and 300 msec (dotted line). B, Control Markov $I_{K,r}$ during AP clamp stimulation at 1000 msec (thick line), 500 msec (thin line), and 300 msec (dotted line).

Table 1. APClamp command protocol morphologies are shown in Figure 2A, and representative control $I_{K,r}$ traces in Figure 2B.

The k_{on} and k_{off} rates for each modifier were chosen such that when stimulated with the voltage step protocol described in Mazhari et al 2001 [9] (V = -80mV for 3 seconds, V = 10mV for 3.5 seconds, V = -50mV for 4 seconds), the IC_{50} (concentration at which peak $I_{K,r}$ is reduced by 50%) of the normalized peak $I_{K,r}$ concentration-response curve for each modifier was 100nM. For each modifier, a sequence of ten increasing concentrations was chosen to produce $I_{K,r}$ block in increasing increments of 10%. See Table 2 for k_{on}, k_{off}, and concentration values.

2.1.3 Generation of synthetic data

In this study, we aimed to reproduce modifier-dependent changes in $I_{K,r}$ during APs at various pacing rates. Therefore, we measured the *in silico* concentration-response of $I_{K,r}$ when

TABLE II
MODIFIER PARAMETERS FOR $MARKOV_{MB}$ MODEL

	$Modifier_{C3}$	$Modifier_O$	$Modifier_I$
K_{on}	0.0360257	0.00013021	5.70106
K_{off}	0.1	0.1	0.1
Conc 1 – 0% $I_{K,r}$ block	0	0	0
Conc 2 – 10% $I_{K,r}$ block	19.3	11.0	11.0
Conc 3 – 20% $I_{K,r}$ block	34.2	24.9	23.8
Conc 4 – 30% $I_{K,r}$ block	51.0	42.7	41.7
Conc 5 – 40% $I_{K,r}$ block	72.0	66.5	65.9
Conc 6 – 50% $I_{K,r}$ block	100	100	100
Conc 7 – 60% $I_{K,r}$ block	141.2	150.3	151.4
Conc 8 – 70% $I_{K,r}$ block	208.8	234.5	237.6
Conc 9 – 80% $I_{K,r}$ block	342.7	403.3	410.5
Conc 10 – 90% $I_{K,r}$ block	742.5	912.6	931.9

Binding rate in $nL \cdot N \cdot molecules^{-1} \cdot ms^{-1}$, unbinding rate in $nL \cdot N \cdot ms^{-1}$, and concentrations in nM for $Modifier_{C3}$, $Modifier_O$, and $Modifier_I$.

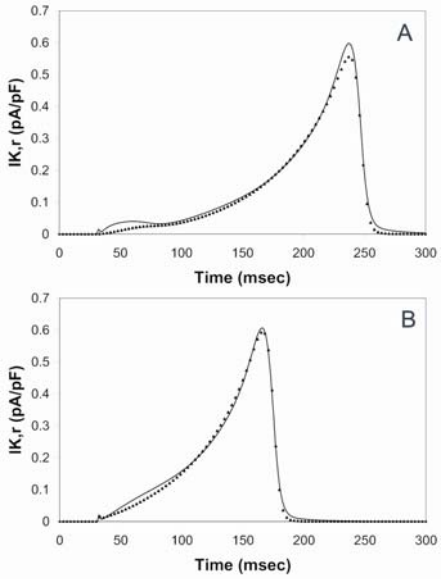

Fig. 3. $I_{K,r}$ traces generated by HH control model (lines) and Markov control model (triangles) in response to an AP clamp. A, CL = 1000 msec. B, CL = 300 msec.

stimulated with an AP clamp protocol. To simulate an AP clamp protocol, steady-state APs from the Hund-Rudy AP model [30] at cycle lengths of 1000, 500, and 300 msec were applied to the model as command potentials (see Appendix A Section A.1.1 for command AP morphologies). Each AP was applied ten times to allow the modifier-$I_{K,r}$ model to reach steady state, and the $I_{K,r}$ trace in response to the final AP at each cycle length was examined.

2.2 Concentration-dependent scaling of Markov model conductance (Markov$_{GKr}$)

In addition to the Markov model with mass action binding presented in Section 2.1.1, this study investigated an alternate method of modeling modifier interaction in a Markov model which involved scaling $I_{K,r}$ conductance (GKr) as a function of concentration. The same control Markov model of $I_{K,r}$ described in Section 2.1.1 was used, and GKr was varied with modifier concentration using the sigmoidal function given in Equation 1:

$$Q(conc) = \frac{Q_0}{1+\left(\frac{conc}{D_{Q,1/2}}\right)^{h_Q}} + \frac{Q_{Inf}}{1+\left(\frac{D_{Q,1/2}}{conc}\right)^{h_Q}} \quad (1)$$

where Q is any given concentration-dependent quantity, conc is the concentration of the modifier in nM, Q_0 is the value of Q when concentration = 0, Q_{Inf} is the value of Q as concentration approaches infinity, $D_{Q,1/2}$ is the value of concentration at which the value of Q = $(Q_0 + Q_{Inf})/2$, and h_Q is the Hill Coefficient, determining the slope of the concentration-response for quantity Q. The four parameters Q_0, Q_{Inf}, $D_{Q,1/2}$, and h_Q for a given quantity Q are collectively referred to as the modifier-effect parameters for that quantity.

The modifier-effect parameters for GKr in the Markov$_{GKr}$ model were then fit to synthetic concentration-response AP clamp data generated by the Markov$_{MB}$ model at the ten modifier concentrations described in Section 2.1.3 using the Levenberg-Marquardt local optimization algorithm [31].

2.3 Hodgkin-Huxley model with modifier effect (HH$_{Mod}$)

We utilized a HH model of $I_{K,r}$ that follows the $I_{K,r}$ formulation given in Hua et al 2004 [29]. This model includes time dependence in both the activation gate (X) and the inactivation gate (Y). The HH model parameters were fit to control AP clamp data generated using the Markov model from section 2.1. The fit was performed using the Levenberg-Marquardt local optimization algorithm [31]. The formulations and parameters for our modified $I_{K,r}$ model are as follows:

$$I_{K,r} = GKr \times X \times Y \times (V - Ek) \quad (2)$$

$$\frac{dX}{dt} = \frac{X^{\infty} - X}{S_x \times \tau_x} \quad (3)$$

$$\frac{dY}{dt} = \frac{Y^{\infty} - Y}{S_Y \times \tau_y} \quad (4)$$

$$X^{\infty} = \frac{1}{1+e^{-(V-R_x)/2.2}} \quad (5)$$

$$\tau_x = 10.1 + \frac{1}{e^{0.103(V-64.6)} + e^{-0.100(V+88.6)}} \quad (6)$$

$$Y^{\infty} = \frac{1}{1+e^{(V-R_Y)/14.8}} \quad (7)$$

$$\tau_y = 0.51 + \frac{1}{e^{1.01(V+31.7)} + e^{-1.00(V+74.3)}} \quad (8)$$

where X and Y are the time- and voltage-dependent open probabilities of activation and inactivation gates, GKr = 0.0502 mS/uF is the conductance of $I_{K,r}$, V is the membrane potential, Ek = -85.6 mV is the reversal potential of the $I_{K,r}$ channel, X^{∞} and Y^{∞} are the steady-state voltage-dependent open probabilities of the activation and inactivation gates, τ_x and τ_y are the voltage-dependent activation and inactivation time constants, R_X and R_Y are the crossover voltages of the steady values for the X and Y gates, and S_X and S_Y are scaling factors for the time constants of the X and Y gates. In the control model, R_X = -68.6 mV, R_Y = -34.1 mV, S_X = 1, and S_Y = 1. $I_{K,r}$ traces generated by the HH model and "target" synthetic data generated by the control Markov simulation in response to an AP clamp at CL = 1000 and 300 msec are shown in Figure 3.

To incorporate the effect of the modifier into the HH model, two alternate strategies were used. First, the effect of the modifier was modeled by allowing channel conductance GKr to vary as a function of concentration according to Equation 1, as described in Section 2.2. If this method was not able to satisfactorily reproduce the $I_{K,r}$ concentration-response target data, several additional model parameters

which describe the functional characteristics of the $I_{K,r}$ channel were allowed to vary as a function of modifier concentration: the crossover voltages of the steady values for the X and Y gates (R_X and R_Y) and scaling factors for the time constants of the X and Y gates (S_X and S_Y). We refer to these four parameters together with GKr as the HH_{Mod} quantities. Each of these quantities was then varied as a function of modifier concentration according to the sigmoidal formulation in Equation 1.

This HH_{Mod} model was then fit to synthetic concentration-response AP clamp data generated by the $Markov_{MB}$ model at the ten modifier concentrations described in Section 2.1.3. To determine the values of the modifier-effect parameters for each HH_{Mod} quantity, a three step process was used. First, the HH_{Mod} quantities themselves were optimized at each concentration, independent of model behavior at any other concentration. The fitted values of a given HH_{Mod} quantity Q at each modifier concentration then form a concentration-response curve for Q. Second, this concentration-response curve for each HH_{Mod} quantity Q was fit using Equation 1 to determine initial values of the modifier-effect parameters Q_0, Q_{Inf}, $D_{Q,1/2}$, and h_Q. Third, the modifier-effect parameters for all of the HH_{Mod} quantities were optimized at the same time to data from all ten concentrations simultaneously. All optimizations were done using the Levenberg-Marquardt optimization algorithm with least squares cost function. The modifier effect parameter values which quantitatively reproduced the $Modifier_{C3}$, $Modifier_I$, and $Modifier_O$ concentration-response of AP clamp $I_{K,r}$ current are given in Table 3, and the averaged least squares costs and optimization times for each parameter set are given in Table 4.

2.4 Whole-cell AP model

To generate predictions about the effect of the theoretical modifiers on APD, we used the most recent canine ventricular AP model that is available, the HRd model of the canine epicardial AP [30]. This model includes several important currents and processes that are absent from earlier canine models, including a formulation of the late sodium current which has been shown to play an important role in heterogeneity of cellular electrical properties [32]. The model is as published except for the following modifications:

TABLE III
MODIFIER-EFFECT PARAMETERS FOR HH_{MOD} MODEL

	Q_0	Q_{inf}	$D_{1/2,Q}$	h_Q
$Modifier_I$				
GKr	0.0502	5.49385e-010	100	0.998918
$Modifier_{C3}$				
GKr	0.0502	0.000982728	12.8282	1.34577
$Modifier_O$				
GKr	0.09369	0.05351	364.652	0.526132
S_X	2.22409	19.1377	803.841	1.1119
S_Y	0.609499	196.466	2033.18	1.37646
R_X	-72.3022	-37.3184	171.548	0.395003
R_Y	-33.9829	48.0234	1957.13	0.655667

TABLE IV
OPTIMIZATION INFORMATION

	Average least squares cost	Computation time (sec)
$Modifier_I$	1.042e-5	1281
$Modifier_{C3}$	1.138e-5	1433
$Modifier_O$	5.605e-5	7756

Average least squares costs and computation times for optimizations of HH_{Mod} model modifier-effect parameters

$[Na^+]_i$,$[K^+]_i$, and $[Cl^-]_i$ were fixed at their steady state values so as to reach steady state more quickly

The original Hund-Rudy $I_{K,r}$ formulation was removed, and replaced with either the Markov model of $I_{K,r}$ described in section 5.1 or the HH model of $I_{K,r}$ described in section 5.2

The model was stimulated with square pulses with duration 1 msec and amplitude 80 mV.

The APs generated by the modified HRd AP models were very similar to those from the original HRd model (Figure 4A).

The HRd model was modified to reproduce midmyocardial (M) ventricular cells (Figure 4B) in the following manner:

$GKs_M = 0.5 * GKs_{Epi}$ as reported in Liu et al 1995 [40]

$GNaL_M = 1.47 * GNaL_{Epi}$ as reported in Zygmunt et al [32]

It has been reported that there is a less than 10% difference between the sodium-calcium exchange current I_{NaCa} in M cells and epicardial cells [41]. Therefore the M cell model used the original I_{NaCa} current model. We note that the results presented in this paper were duplicated using the ten Tusscher human AP model [33] (data not shown), and were found to be independent of the choice of AP model.

The existing $I_{K,r}$ component of HRd was replaced with either the $Markov_{MB}$ $I_{K,r}$ model described in Section 2.1, the $Markov_{GKr}$ $I_{K,r}$ model described in Section 2.2, or the HH_{Mod} $I_{K,r}$ model described in Section 2.3, and steady-state APD_{90} was measured at various pacing cycle lengths. In the absence of any modifier effects (concentration = 0), all of the substituted $I_{K,r}$ HRd models produce APs similar to the original HRd. Each of the substituted $I_{K,r}$ HRd models was also modified to qualitatively reproduce the behavior of midmyocardial myocytes.

2.4 Simulation details

All simulations and optimizations were run on a Dell Inspiron 9100 computer using custom written C++ computer code. Each ionic model as described above (either single channel or whole-cell) is represented by a set of differential equations of the form $dx/dt = f(x,t,p)$, where x is a vector describing the current state of the system, t is time, and p is a vector of parameters. For the models described, the corresponding differential equations are usually quite stiff in the sense that they have widely separated time scales: some variables change rapidly under small perturbations while others change slowly. To improve the accuracy of our simulations, we used the CVODES package from Lawrence Livermore National Laboratories [34] with the backwards

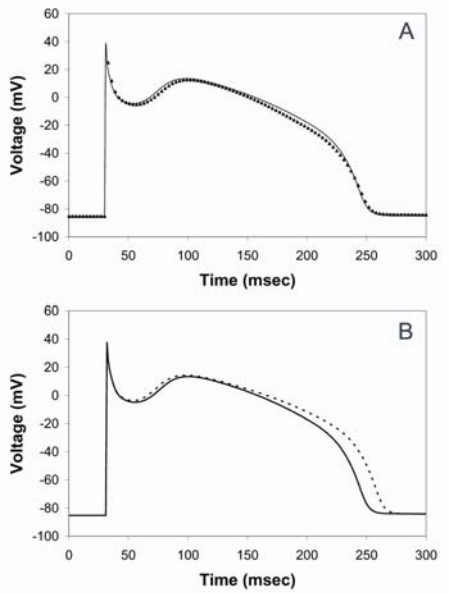

Fig. 4. A, Simulated APs at 1000 msec generated using original HRd model (triangles) and $Markov_{MB}$ substituted $I_{K,r}$ HRd model (solid line). B, Simulated epicardial (solid line) and midmyocardial (dotted line) APs at 1000 msec generated using the control HH_{Mod} IK,r model in the HRd AP model.

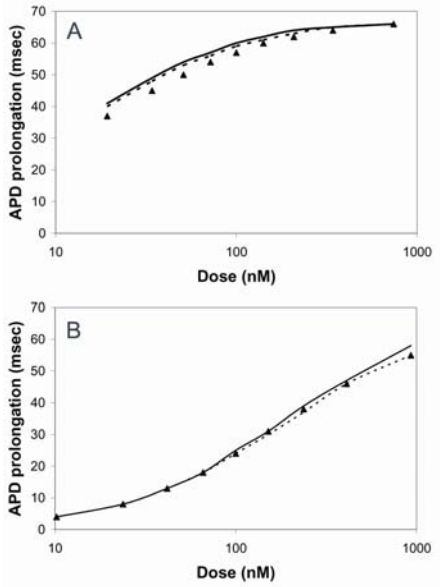

Fig. 5. APD prolongation concentration-response predictions generated by $Markov_{MB}$ (triangles), $Markov_{GKr}$ (dotted lines), and HH_{Mod} (solid lines), paced at CL = 1000 msec. A, $Modifier_{C3}$. B, $Modifier_I$.

differentiation formula, which is designed for stiff systems. We also used automatic differentiation to calculate the jacobian derivative of the function f for use with the dense Newton based solver that is included as part of CVODES.

For the optimization of models to data, we used the Levenberg-Marquardt local optimizer [31]. The cost for a particular simulation is based on a sum of squares calculation. At each time point for which there is experimental data, the difference between the simulation value and the experimental value is squared. These squares are then summed over all the data points, and the sum represents the cost for that simulation. The optimization problem consists of finding parameters to minimize the cost.

III. Results

3.1 APD concentration-response predictions

To evaluate the simplifications involved in the $Markov_{GKr}$ and HH_{Mod} models relative to the $Markov_{MB}$ model, we examined predictions of APD concentration-response based on $I_{K,r}$ ion current data for theoretical modifiers binding the C_3, O, and I states of the $Markov_{MB}$ model. To assess the ability of the models to accurately capture rate-dependent effects, three cycle lengths were studied (CL=1000, 500, and 300 msec).

As Figure 5 shows, all three methods produced quantitatively equivalent APD concentration-response predictions for $Modifier_I$ and $Modifier_{C3}$ at a pacing interval of 1000msec. This result is consistent with those at pacing intervals of 500 msec and 300 msec (data not shown).

As Figure 6 shows, the APD concentration-response predictions for $Modifier_O$ at pacing intervals of 1000 msec and 300 msec generated by the $Markov_{GKr}$ method captured the qualitative trend in the $Markov_{MB}$ predictions, but were not quantitatively equivalent, whereas the HH_{Mod} predictions were quantitatively equivalent to the $Markov_{MB}$ model for $Modifier_O$. These results are consistent with those seen at a pacing interval of 500 msec (data not shown). The agreement between HH_{Mod} and $Markov_{MB}$ predictions across pacing cycle length indicate that the HH_{Mod} model was able to reproduce the rate-dependence of $Modifier_O$ seen in $Markov_{MB}$.

3.2 $I_{K,r}$ morphology concentration-response predictions

To explore the failure of $Markov_{GKr}$ to quantitatively reproduce the $Markov_{MB}$ APD concentration-response predictions for $Modifier_O$, we examined the concentration-dependent changes in $I_{K,r}$ morphology for $Modifier_O$ in each of the three models.

As Figure 7A shows, the morphology of the $Markov_{MB}$ $I_{K,r}$ current changes as a function of $Modifier_O$ concentration in a nontrivial manner. As concentration increases, $I_{K,r}$ during repolarization decreases more quickly than $I_{K,r}$ during the AP plateau. Additionally, $I_{K,r}$ during the upstroke and notch increases with concentration at shorter cycle lengths. The HH_{Mod} model of the effect of the modifier displays these concentration-dependent behaviors in $I_{K,r}$ morphology (Figure 7B). In contrast, the $Markov_{GKr}$ model cannot capture morphological changes in $I_{K,r}$ (Figure 7C) because the $Markov_{GKr}$ model is limited to scaling the amplitude of the $I_{K,r}$ current. A comparison of the $I_{K,r}$ traces of the three models at a high concentration of $Modifier_O$ (Figure 7D) clearly demonstrates these morphological differences.

The changes in $I_{K,r}$ morphology caused by a modifier that binds the open state of the channel have a significant effect on APD (Figure 6). This result is of particular interest given that

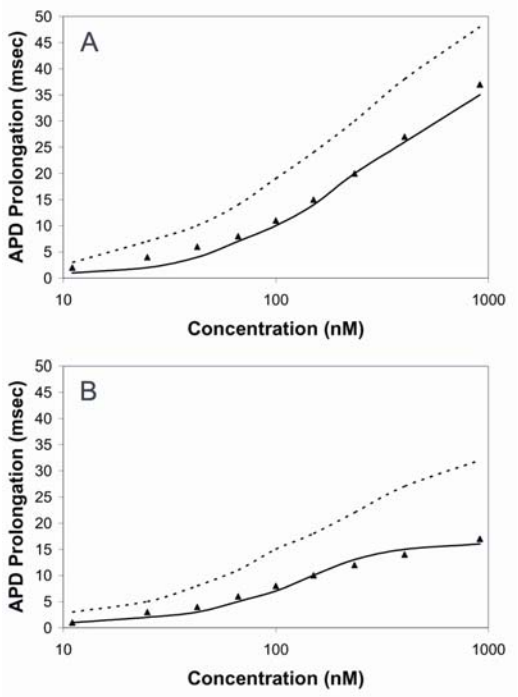

Fig. 6. APD prolongation concentration-response predictions for $Modifier_O$ generated by $Markov_{MB}$ (triangles), $Markov_{GKr}$ (dotted lines), and HH_{Mod}. A, CL = 1000 msec. B, CL = 300 msec.

several modifiers (e.g. MK-499 [35], E4031 [35], almokalant [36], dofetilide [37, 38], and ibutilide [37]), are known to bind the open state of the $I_{K,r}$ channel.

3.3 Insights into functional differences between modifiers binding different conformational states of $I_{K,r}$

Examination of the simulation results and of the parameters in the HH_{Mod} model allows one to connect the physical interaction of a modifier with the HERG channel to its functional effect on the $I_{K,r}$ current, providing insight into how the results obtained in the HH model reflect the molecular mechanisms in the $Markov_{MB}$ model. As shown in Table 3, reproducing the concentration-response behavior of $Modifier_O$ required concentration-dependent changes in $I_{K,r}$ channel kinetics ($Q_0 \neq Q_{Inf}$ for all HH_{Mod} quantities) as well as concentration-dependent reduction of the $I_{K,r}$ amplitude. The binding of $Modifier_O$ resulted in an increase in the activation and inactivation time constants, and positive shifts in the steady-state crossover voltages of both activation and inactivation gates. Conversely, reducing $I_{K,r}$ amplitude without affecting channel kinetics was sufficient to reproduce the concentration-response behaviors of $Modifier_{C3}$ and $Modifier_I$. The difference in GKr $D_{1/2,Q}$ values between $Modifier_{C3}$ and $Modifier_I$ indicates that although both modifiers had a similar qualitative effect on $I_{K,r}$, and both had the same IC_{50} of 100nM in response to stimulation with a voltage step protocol, the two modifiers had significantly different effective IC_{50} values in the AP model. This discrepancy is due to differences in state occupancy dynamics during stimulation with a voltage step protocol versus

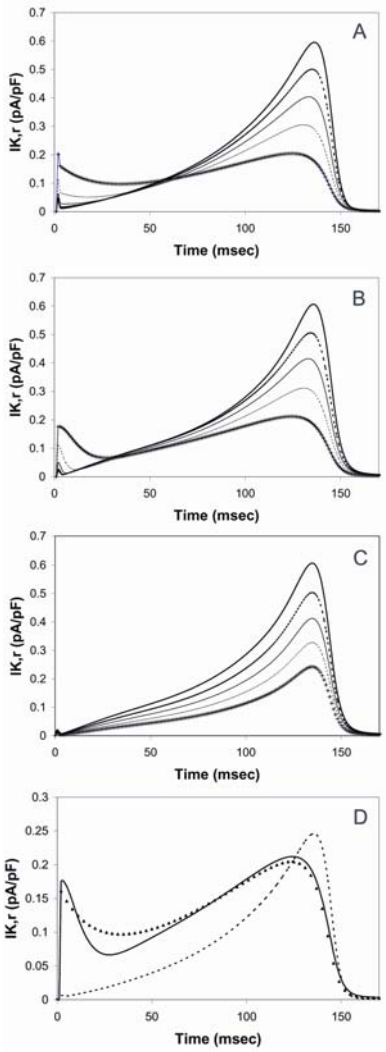

Fig. 7. $I_{K,r}$ in response to AP clamp stimulation paced al CL = 300 msec, with $Modifier_O$ = 0 nM (thick solid lines), 25 nM (thick dotted lines), 67 nM (thin solid lines), 150 nM (thin dotted lines), 403 nM (pluses). A, $Markov_{MB}$. B, HH_{Mod}. C, $Markov_{GKr}$. D, Comparison of $Markov_{MB}$ (triangles), $Markov_{GKr}$ (dotted lines), and HH_{Mod} (solid lines) at $Modifier_O$ = 234 nM.

unclamped AP pacing, as described below.

Examination of $Markov_{MB}$ state occupancy probability densities can help elucidate the mechanisms of these functional differences in the effect of the modifier. At rest, the probability density on state C_1 is larger than that of any other state (probability density is localized on C_1). When membrane voltage is increased, either during AP upstroke or voltage step from -80mV to 10mV, the probability density shifts from localization on C_1 to I, transitioning mainly via C_3 to I inactivation, producing only slight O occupancy and therefore little $I_{K,r}$ current. When membrane voltage is then decreased, either during repolarization or voltage step to -50mV, probability density shifts from I back to C_1, via both the I to O transition and the I to C_3 transition, producing significant transient O state occupancy and $I_{K,r}$ current.

In the presence of $Modifier_{C3}$, modifier binding occurs when probability density is localized on state C_3, largely

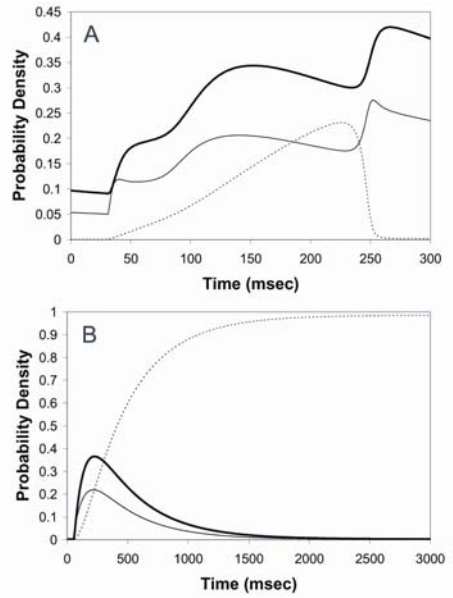

Fig. 8. $Markov_{MB}$ $I_{K,r}$ state occupancy probability density of states C_3 (thin solid line), $C_{3,Bound}$ (thick solid line), and I (dotted line), with $Modifier_{C3}$ = 5nM. A, during AP clamp at CL = 1000msec. B, during voltage step from -80mV to 10mV.

during the inactivation transition from C_1 to I via C_3 (Figure 8A). This binding reduces the probability density of state I during inactivation, and therefore decreases transient density flow through state O during repolarization, thereby decreasing $I_{K,r}$ current. However, while the membrane voltage is held at 10mV in the voltage step protocol, probability density gradually transitions from the C_3-bound state to state I (Figure 8B), thereby reducing the effect of $Modifier_{C3}$ on $I_{K,r}$. This causes long voltage step protocols to underestimate the effect $Modifier_{C3}$ will have on $I_{K,r}$ during APs. Conversely, since probability density is localized on state I immediately prior to the voltage step from 10mV to -50mV and the subsequent occurrence of the $I_{K,r}$ transient, the effect of $Modifier_I$ on $I_{K,r}$ during APs is accurately captured by such voltage step protocols.

In the presence of $Modifier_O$, some probability density is localized on the O_{Bound} state throughout the action potential and during the rest interval, particularly at high concentrations and rapid pacing rates. During the AP upstroke and plateau, a fraction of this probability density transitions from O_{Bound} to I via O, resulting in increased early $I_{K,r}$. During repolarization, however, the significant fraction of channels in the O_{Bound} state reduces the probability density localized on O, resulting in less late $I_{K,r}$ (Figure 9A).

Reproduction of this biphasic response of $I_{K,r}$ to $Modifier_O$ requires a modification of the kinetics of $I_{K,r}$ in addition to the maximal conductance GKr. In the Hodgkin-Huxley model of $I_{K,r}$, increasing τ_Y and R_Y results in a greater inactivation gate open probability during upstroke and plateau, and lower open probability during repolarization and rest (Figure 9B, solid lines). Increasing τ_X and R_X causes an accumulation of activation gate open probability, particularly at high concentrations and fast pacing rates, resulting in an

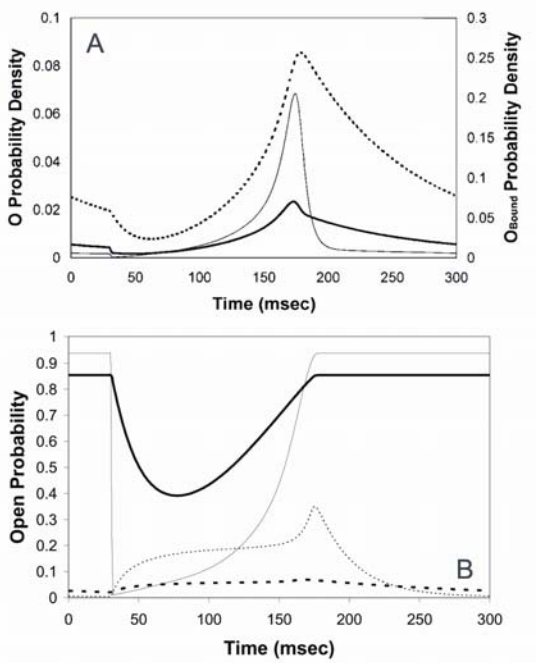

Fig. 9. A, $Markov_{MB}$ $I_{K,r}$ in response to AP clamp CL = 300 msec. State occupancy probability densities of state O (control, thin solid line; $Modifier_O$ = 200 nM, thin dotted line) and O_{Bound} ($Modifier_O$ = 200 nM, thick solid line). B, HH_{Mod} $I_{K,r}$ in response to AP clamp CL = 300 msec. Open probabilities for activation gate X (control, thin dotted line; ModifierO = 1000 nM, thick dotted line) and inactivation gate Y (control, thin solid line; ModifierO = 1000 nM, thick solid line).

increase in $I_{K,r}$ during the upstroke and early plateau. The same changes in activation kinetics result in a decrease in open probability, and therefore less current, during repolarization (Figure 9B, dotted lines). These effects, combined with a decrease in GKr, result in the biphasic $I_{K,r}$ $Modifier_O$ concentration-response exhibited by $Markov_{BD}$.

3.4 Intrinsic electrical heterogeneity concentration-response predictions

To examine predictions about the effect of the modifier on intrinsic electrical heterogeneity, the HRd AP model, originally designed to describe epicardial (EPI) myocytes, was modified to qualitatively reproduce the behavior of midmyocardial myocytes (M) [26]. See Appendix A Section A.3 for AP model details and morphologies. The APD concentration-response predictions for $Modifier_O$ generated by $Markov_{MB}$, $Markov_{GKr}$ and HH_{Mod} in these two AP models were then studied. Because preferential prolongation of M cell APD is thought to be arrhythmogenic, we investigated each method's prediction of concentration-dependent changes in the difference between M cell APD (APD_M) and EPI cell APD (APD_{Epi}).

The HH_{Mod} model reproduced heterogeneity concentration-response predictions for $Modifier_O$ generated by the $Markov_{MB}$ model in a quantitative manner, whereas $Markov_{GKr}$ did so only qualitatively (Figure 10). Simulations at cycle lengths of 500 and 300 msec produced similar results (data not shown).

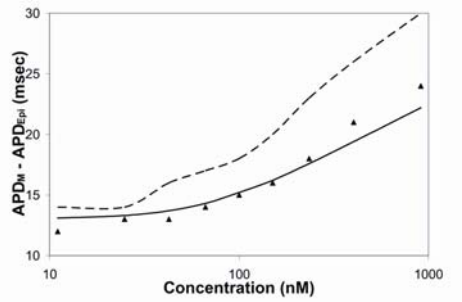

Fig. 10. (APD_M-APD_{Epi}) concentration-response for $Modifier_O$ at a cycle length of 1000 msec generated by HRd cell model using $Markov_{MB}$ (triangles), $Markov_{GKr}$ (dashed line), and HH_{Mod} (solid line).

The simulations also suggest a mechanism for preferential prolongation of M cell APD. In the absence of any modifier, the AP plateau voltage is higher in M cells than in epicardial cells, due to less $I_{K,s}$ outward current and more $I_{Na,L}$ inward current. The higher voltage causes an approximately 10% larger driving force (V - Ek) at the time of peak $I_{K,r}$, and results in an approximately 10% larger peak $I_{K,r}$ current in M cells than in epicardial cells. Therefore, decreasing $I_{K,r}$ in M cells has a more significant prolonging effect on APD than in EPI cells.

3.5 APD concentration-response predictions in the presence of Gaussian noise

To evaluate the effectiveness of the HH_{Mod} model and the optimization strategy described in Section 2.4 for reproducing experimental data, Gaussian noise was added to the synthetic data for $Modifier_O$. The mean of the noise was set to 0 and the standard deviation was estimated to be to 0.046 pA/pF from experimental $I_{K,r}$ recordings [29]. Four sets of APD concentration-response predictions for ModifierO were generated by fitting to four replicates of $I_{K,r}$ concentration-response data with random noise. As Figure 11 shows, the addition of noise did not significantly effect the HH_{Mod} APD concentration-response predictions.

IV. Discussion

In this study, we used mathematical models to investigate strategies for using ion current data to predict the effect of channel-binding chemical species on cellular properties such as APD and intrinsic electrical heterogeneity. Our study focused on the delayed rectifier K^+ current $I_{K,r}$ due to the link between $I_{K,r}$ block, prolonged APD, amplified intrinsic electrical heterogeneity, and susceptibility to arrhythmias [26], but the methods developed here should be generally applicable to other electrophysiological studies. We compared three methods for quantifying modifier-ion current interactions and generating cellular APD concentration-response predictions that appear to offer the typical trade-offs between computational efficiency and accuracy of prediction. The results of our simulations suggest a mathematical modeling strategy for characterizing the effect of modifier-ion current interactions on cellular electrophysiological properties

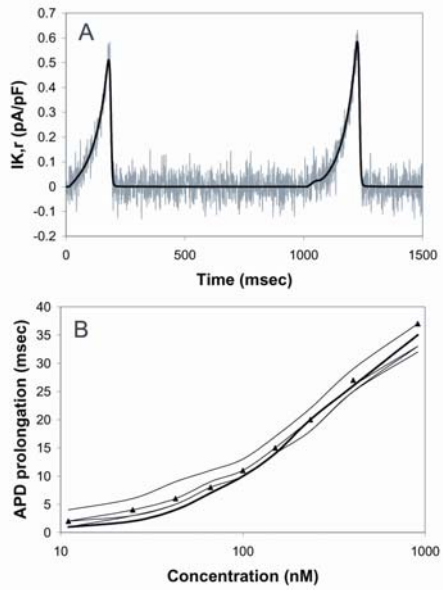

Fig. 11. A, Untransformed control $Markov_{MB}$ $I_{K,r}$ trace (black line) and the same trace with one replicate of Gaussian noise added. B, $Modifier_O$ APD concentration-response predictions at CL = 1000 msec generated by $Markov_{MB}$ (triangles), HH_{Mod} without noise (thick line), and four replicates of HH_{Mod} with added noise (thin lines).

that can quantitatively reproduce behaviors from a more computationally demanding approach.

The most complex approach we studied was to model the modifier-ion current interaction through simulation of the physical interaction of the modifier with the channel protein using a Markov model with mass action binding. Such a model can capture a range of dynamic behaviors, and can provide physiological insight into the modifier's mechanism of action. However, if the binding properties of a modifier are unknown, then estimating parameters for the transition rates between all possible bound states is necessary. This method would require the estimation of a large number of parameters simultaneously, which is very computationally expensive. Therefore, a simplified and more computationally efficient method is desirable.

The simplest approach for modeling modifier-ion current interactions that we studied was to scale conductance as a function of modifier concentration. While using this approach in a Markov model qualitatively reproduced the APD concentration-response predictions generated by a Markov model with explicit modifier binding for three theoretical modifiers, scaling the conductance did not quantitatively reproduce the predictions for the open channel binding modifier. Additionally, scaling conductance generated predictions about the effect of the modifier on heterogeneity that were qualitatively, but not quantitatively, consistent with those made by the $Markov_{MB}$ model. Therefore, we conclude that for applications that do not require quantitative accuracy, scaling channel conductance is as effective as mass action binding for modeling modifier-ion current interactions. The main advantage of the conductance scaling modeling strategy over others is its simplicity: only four parameters need to be

estimated. However, for applications where both computational efficiency and quantitative accuracy are necessary, neither of the above approaches is adequate.

We have shown that a Hodgkin-Huxley model of $I_{K,r}$ in which important kinetic parameters are defined as concentration-dependent can quantitatively reproduce the cellular APD concentration-response predictions for several theoretical modifiers generated by a Markov model of $I_{K,r}$ with mass action binding. By fitting the ion current time series generated in response to an AP clamp at three cycle lengths, the HH_{Mod} model was able to reproduce the $Markov_{MB}$ concentration-response predictions of $I_{K,r}$ morphology, APD, and heterogeneity. The HH_{Mod} method presented here has computational advantages over Markov models with mass action binding. The HH_{Mod} method requires no prior knowledge about the modifier's mechanism of action and binding kinetics. Clearly, this is of great importance when studying novel modifiers. The HH_{Mod} method requires the estimation of 21 parameters, which is a more tractable optimization problem than that offered by the $Markov_{MB}$ model, particularly when approached in the three-stage manner described in Section 2.3.

Such a model of modifier effect on $I_{K,r}$ could aid researchers in predicting the effect of novel ion current modifiers on cellular and tissue properties. Experimental concentration-response data describing the effect of a novel modifier on $I_{K,r}$ could be collected, and then the HH modifier-effect model optimized to reproduce the experimental data, as described in Section 2.3. This optimized model could then be incorporated into a whole cell AP model, as described in Section 2.4, and used to generate predictions about the effect of the modifier on cellular properties such as action potential duration. Furthermore, the new AP model could then be integrated into a multi-cell, tissue level model to generate predictions about the effect of the modifier on tissue level properties, such as wave propagation and arrhythmogenesis.

These results suggest promising directions for future experimental work. A logical extension of this study would involve experimental validation of the approach presented here. Experimental data for modifiers binding $I_{K,r}$ could be fit using the HH_{Mod} method, and the model predictions for APD concentration-response checked against experimental results, allowing assessment of the reliability of this method of modeling modifier effect. In addition, the simulation results suggest that voltage step protocols are not ideal for measuring the effect of the modifier on $I_{K,r}$ during APs, and that development of a more predictive command protocol would be desirable. These efforts will likely benefit from an approach that uses computational methods similar to those presented in this study to help guide experimental design and interpret results.

Although the method presented here reproduced the APD concentration-response data generated using a Markov model with mass action binding, there were several limitations to our study. First, this study only examined modeling of modifier interaction with I_{Kr} and did not address the development of the control model of the current. However, preliminary tests indicate that the results do not depend sensitively on the control model parameters; several different low cost control Hodgkin-Huxley parameter sets produced very similar results. Secondly, several simplifying assumptions were used to model modifier binding in the Markov model, such as ignoring explicit voltage-dependence of binding and the spatial distribution of modifier molecules. In addition, it is known that drugs such as cisapride bind more than one state of the HERG channel[39], and this study did not thoroughly explore modifiers that bind multiple states of the channel. However, the HH_{Mod} model was able to quantitatively replicate $Markov_{MB}$ APD concentration-response predictions for several theoretical compounds that bind more than one conformational state (data not shown), including non-monotonic concentration-dependent changes in peak $I_{K,r}$ and APD. In addition, this method could be used in conjunction with a Markov model to develop a thorough understanding of a modifier's mechanism of action and the connection between its binding properties and their functional consequences.

In conclusion, we have proposed a Hodgkin-Huxley based modeling method that is as predictive as a more complex Markov formulation and reveals the functional effect of modifier-ion current interactions, but that requires no prior knowledge of binding dynamics and fewer computational resources. This method could allow researchers to more easily generate predictions about the effect of novel ion current modifiers on cellular and tissue properties. Such a computational approach could be a powerful tool to help researchers connect the molecular effects of signaling pathways and channel blockers to changes in cellular and tissue behaviors.

ACKNOWLEDGMENT

We thank Dr. Robert F. Gilmour Jr. for insightful comments and suggestions, as well as our colleagues at Gene Network Sciences for their invaluable contributions, in particular Moses Wilks for assistance with simulations and Robert Miller and Basudev Chaudhuri for help with Visual Cell software.

REFERENCES

[1] A. L. Hodgkin and A. F. Huxley, "A quantitative description of membrane current and its application to conduction and excitation in nerve," *J Physiol,* vol. 117, pp. 500-544, 1952.

[2] B. Hille, *Ionic Channels of Excitable Membranes*. Sunderland, Mass.: Sinauer Associates, Inc., 1992.

[3] Y. Kurata, I. Hisatome, S. Imanishi, and T. Shibamoto, "Roles of L-type Ca2+ and delayed-rectifier K+ currents in sinoatrial node pacemaking: insights from stability and bifurcation analyses of a mathematical model.," *Am J Physiol Heart Circ Physiol,* vol. 285, pp. 2804-2819, 2003.

[4] G. B. Ermentrout and C. C. Chow, "Modeling neural oscillations," *Physiol Behav,* vol. 77, pp. 629-633, 2002.

[5] J. Jo, H. Kang, M. Y. Choi, and D. S. Koh, " How noise and coupling induce bursting action potentials in pancreatic {beta}-cells," *Biophys J.,* vol. 89, pp. 1534-1542, 2005.

[6] C. H. Luo and Y. Rudy, "A model of the ventricular cardiac action potential. Depolarization, repolarization, and their interaction," *Circ Res,* vol. 68, pp. 1501-26, Jun 1991.

[7] D. DiFrancesco and D. Noble, "A model of cardiac electrical activity incorporating ionic pumps and concentration changes," *Philos Trans R Soc Lond B Biol Sci,* vol. 307, pp. 353-98, Jan 10 1985.

[8] J. P. Keener and J. Sneyd, *Mathematical Physiology*. New York: Springer, 1998.

[9] R. Mazhari, J. L. Greenstein, R. L. Winslow, E. Marban, and H. B. Nuss, "Molecular interactions between two long-QT syndrome gene products, HERG and KCNE2, rationalized by in vitro and in silico analysis," *Circ Res,* vol. 89, pp. 33-8, Jul 6 2001.

[10] E. X. Albuquerque, J. W. Daly, and J. E. Warnick, "Macromolecular sites for specific neurotoxins and drugs on chemosensitive synapses and electrical excitation in biological membranes," *Ion Channels,* vol. 1, pp. 95-162, 1988.

[11] R. Malek, K. K. Borowicz, Z. Kimber-Trojnar, G. Sobieszek, B. Piskorska, and S. J. Czuczwar, "Remacemide--a novel potential antiepileptic drug," *Pol J Pharmacol,* vol. 55, pp. 691-698, 2003.

[12] T. J. Kamp and J. W. Hell, "Regulation of cardiac L-type calcium channels by protein kinase A and protein kinase C," *Circ Res,* vol. 87, pp. 1095-102, Dec 8 2000.

[13] H. L. Tan, S. Kupershmidt, R. Zhang, S. Stepanovic, D. M. Roden, A. A. M. Wilde, M. E. Anderson, and J. R. Balser, "A calcium sensor in the sodium channel modulates cardiac excitability," *Nature,* vol. 415, pp. 442-447, JAN 24 2002.

[14] J. Cui, Y. Melman, E. Palma, G. I. Fishman, and T. V. McDonald, "Cyclic AMP regulates the HERG K^+ channel by dual pathways," *Curr Biol,* vol. 10, pp. 671-4, Jun 1 2000.

[15] W. Haverkamp, G. Breithardt, A. J. Camm, M. J. Janse, M. R. Rosen, C. Antzelevitch, D. Escande, M. Franz, M. Malik, A. Moss, and R. Shah, "The potential for QT prolongation and pro-arrhythmia by non-anti-arrhythmic drugs: clinical and regulatory implications. Report on a Policy Conference of the European Society of Cardiology," *Cardiovasc Res,* vol. 47, pp. 219-33, Aug 2000.

[16] J. S. Mitcheson, J. Chen, M. Lin, C. Culberson, and M. C. Sanguinetti, "A structural basis for drug-induced long QT syndrome," *Proc Natl Acad Sci U S A,* vol. 97, pp. 12329-33, Oct 24 2000.

[17] B. Fermini and A. A. Fossa, "The impact of drug-induced QT interval prolongation on drug discovery and development," *Nat Rev Drug Discov,* vol. 2, pp. 439-47, Jun 2003.

[18] C. Antzelevitch, L. Belardinelli, A. C. Zygmunt, A. Burashnikov, J. M. Di Diego, J. M. Fish, J. M. Cordeiro, and G. Thomas, "Electrophysiological effects of ranolazine, a novel antianginal agent with antiarrhythmic properties," *Circulation,* vol. 110, pp. 904-10, Aug 24 2004.

[19] D. Bottino, R. C. Penland, A. Stamps, M. Traebert, B. Dumotier, A. Georgieva, G. Helmlinger, and G. S. Lett, "Preclinical cardiac safety assessment of pharmaceutical compounds using an integrated systems-based computer model of the heart.," *Progress in Biophysics & Molecular Biology,* vol. 90, pp. 414-443, July 7 2005.

[20] J. M. Ridley, J. T. Milnes, Y. H. Zhang, H. J. Witchel, and H. J.C., "Inhibition of HERG K+ current and prolongation of the guinea-pig ventricular action potential by 4-aminopyridine.," *The Journal of Physiology,* vol. 549, pp. 667-672, June 15 2003.

[21] A. Zaza, M. Micheletti, A. Brioschi, and M. Rocchetti, "Ionic currents during sustained pacemaker activity in rabbit sino-atrial myocytes.," *The Journal of Physiology,* vol. 505, pp. 677-88, Dec 15 1997.

[22] G. J. Amos, I. Jacobson, G. Duker, and L. Carlsson, "Block of HERG-carried K+ currents by the new repolarization delaying agent H 345/52.," *Journal of Cardiovascular Electrophysiology,* vol. 14, pp. 651-658, June 2003.

[23] T. Doerr, R. Denger, and W. Trautwein, "Calcium currents in single SA nodal cells of the rabbit heart studied with action potential clamp.," *Pflugers Archiv : European journal of physiology.,* vol. 413, pp. 599-603, April 1989.

[24] G. E. Kirsch, E. S. Trepakova, J. C. Brimecombe, S. S. Sidach, H. D. Erickson, M. C. Kochan, L. M. Shyjka, A. E. Lacerda, and A. M. Brown, "Variability in the measurement of hERG potassium channel inhibition: effects of temperature and stimulus pattern," *J Pharmacol Toxicol Methods,* vol. 50, pp. 93-101, Sep-Oct 2004.

[25] L. A. Irvine, M. S. Jafri, and R. L. Winslow, "Cardiac sodium channel Markov model with temperature dependence and recovery from inactivation," *Biophys J,* vol. 76, pp. 1868-85, Apr 1999.

[26] J. M. Di Diego, L. Belardinelli, and C. Antzelevitch, "Cisapride-induced transmural dispersion of repolarization and torsade de pointes in the canine left ventricular wedge preparation during epicardial stimulation," *Circulation,* vol. 108, pp. 1027-33, Aug 26 2003.

[27] C. F. Starmer, A. Grant, and H. C. Strauss, "Mechanisms of use-dependent block of sodium channels in excitable membranes by local anesthetics.," *Biophysical Journal,* vol. 46, pp. 15-17, July 1984.

[28] F. R. Gilliam, C. F. Starmer, and A. O. Grant, "Blockade of rabbit atrial sodium channels by lidocaine. Characterization of continuous and frequency-dependent blocking.," *Circ Res,* vol. 65, pp. 723-39, Sep 1989.

[29] F. Hua and R. F. Gilmour, Jr., "Contribution of IKr to rate-dependent action potential dynamics in canine endocardium," *Circ Res,* vol. 94, pp. 810-9, Apr 2 2004.

[30] T. J. Hund and Y. Rudy, "Rate dependence and regulation of action potential and calcium transient in a canine cardiac ventricular cell model," *Circulation,* vol. 110, pp. 3168-74, Nov 16 2004.

[31] D. Marquardt, "An Algorithm for Least-Squares Estimation of Nonlinear Parameters.," *Siam Journal on Applied Mathematics,* vol. 11, pp. 431-441, 1963.

[32] A. C. Zygmunt, G. T. Eddlestone, G. P. Thomas, V. V. Nesterenko, and C. Antzelevitch, "Larger late sodium conductance in M cells contributes to electrical heterogeneity in canine ventricle," *Am J Physiol,* vol. 281, pp. H689-97, Aug 2001.

[33] K. H. ten Tusscher, D. Noble, P. J. Noble, and A. V. Panfilov, "A model for human ventricular tissue," *Am J Physiol Heart Circ Physiol,* vol. 286, pp. H1573-89, Apr 2004.

[34] S. D. Cohen and A. C. Hindmarsh, "CVODE User Guide," *LLNL Report,* vol. UCRL-MA-118618, October 1994.

[35] P. S. Spector, M. E. Curran, M. T. Keating, and M. C. Sanguinetti, "Class III antiarrhythmic drugs block HERG, a human cardiac delayed rectifier K+ channel. Open-channel block by methanesulfonanilides," *Circ Res,* vol. 78, pp. 499-503, Mar 1996.

[36] E. Carmeliet, "Use-dependent block and use-dependent unblock of the delayed rectifier K+ current by almokalant in rabbit ventricular myocytes.," *Circ Res,* vol. 73, pp. 857-868, 1993.

[37] T. Yang, M. S. Wathen, A. Felipe, M. M. Tamkun, D. Snyders, and D. Roden, "K+ currents and K+ channel mRNA in cultured atrial cardiac myocytes (AT-1 cells)." *Circ Res,* vol. 75, pp. 870-878, 1994.

[38] E. Carmeliet, "Voltage- and time-dependent block of the delayed rectifier K+ current in cardiac myocytes by dofetilide.," *J Pharmacol Exp Ther,* vol. 262, pp. 809-817, 1992.

[39] B. D. Walker, C. B. Singleton, J. A. Bursill, K. R. Wyse, S. M. Valenzuela, M. R. Qiu, S. N. Breit, and T. J. Campbell, "Inhibition of the human ether-a-go-go-related gene (HERG) potassium channel by cisapride: affinity for open and inactivated states," *Br J Pharmacol,* vol. 128, pp. 444-50, Sep 1999.

[40] D. W. Liu and C. Antzelevitch, "Characteristics of the delayed rectifier current (I_{Kr} and I_{Ks}) in canine ventricular epicardial, midmyocardial, and endocardial myocytes. A weaker I_{Ks} contributes to the longer action potential of the M cell," *Circ Res,* vol. 76, pp. 351-65, Mar 1995.

[41] A. C. Zygmunt, R. J. Goodrow, and C. Antzelevitch, "I_{NaCa} contributes to electrical heterogeneity within the canine ventricle," *Am J Physiol,* vol. 278, pp. H1671-8, May 2000.